

ORBIT MAINTENANCE STRATEGY FOR EARTH-MOON HALO ORBITS

Vivek Muralidharan* and Kathleen C. Howell†

The L1 and L2 Near Rectilinear Halo Orbits (NRHOs) are proposed long horizon trajectories for cislunar exploration missions. Due to unmodeled forces as well as orbit determination errors in this dynamically sensitive region, the spacecraft deviates from the desired path. The current investigation focuses on an extended analysis of an impulsive stationkeeping technique to maintain the spacecraft near a long horizon virtual reference orbit. The dynamics in the halo orbit region are explored to identify suitable maneuver and target locations for stationkeeping. Furthermore, phasing constraints are incorporated to maintain spacecrafts on orbit where position and velocity states are sensitive to epoch time.

INTRODUCTION

Long term cislunar mission scenarios are the current priority for many space organizations. Near rectilinear halo orbits (NRHOs) are members of the family of halo orbits in the L1 and L2 regions of the Earth-Moon system that offer potential candidates suitable for any long term presence. These NRHOs are stable or nearly stable as characterized by the linear variational flow in the circular restricted three-body problem (CR3BP).^{1,2} The near rectilinear halo orbits offer reasonably close lunar passages and large out-of-plane amplitudes relative to the Earth-Moon orbit plane, appropriate for investigating the polar regions of the Moon.

The NRHOs are periodic in the circular restricted three-body problem, however, in the higher-fidelity ephemeris model, these orbits are no longer closed, but quasi-periodic. The additional forces beyond those in the CR3BP model adds complexity to the dynamics in the vicinity of the NRHOs. The current investigation explores a systematic and straightforward approach to select parameters suitable for an impulsive stationkeeping scheme to overcome position and velocity uncertainties in orbit determination as well as any unmodeled errors.

Existing strategies that are based on manifold theory, such as Floquet mode approach,³⁻⁵ cannot generally be leveraged for stationkeeping in support of activities in stable or nearly stable orbits that do not possess well-distinguished stable and unstable manifolds. A technique commonly identified as an x -axis control strategy that exploits some near symmetry of the orbits is sometimes employed for stationkeeping in the cislunar region, including the near rectilinear halo orbits.^{2,6-10} The performance of the impulsive stationkeeping technique is subject to the location of the maneuvers, the time duration between two successive maneuvers as well as the target horizon time. The current investigation aids in selecting combinations of these three factors suitable for successful orbit maintenance.

*Ph.D. Candidate, School of Aeronautics and Astronautics, Purdue University, Neil Armstrong Hall of Engineering, 701 W. Stadium Ave., West Lafayette, IN 47907, muralidv@purdue.edu

†Hsu Lo Distinguished Professor of Aeronautics and Astronautics, School of Aeronautics and Astronautics, Purdue University, Neil Armstrong Hall of Engineering, 701 W. Stadium Ave., West Lafayette, IN 47907, howell@purdue.edu

Certain members of the halo orbit families are particularly sensitive to epoch dates with distinct characteristics in the higher-fidelity ephemeris model in comparison to the CR3BP counterpart. As a result, targeting conditions that are not synchronized in phase are observed to be ineffective in stationkeeping. The influence of additional phase constraints for stationkeeping is investigated.

BACKGROUND: NEAR RECTILINEAR HALO ORBITS

The circular restricted three-body problem (CR3BP) is a time invariant approximation for the spacecraft dynamics in the higher-fidelity ephemeris model. The CR3BP model characterizes the motion of a spacecraft influenced by the gravitational forces of two primary bodies, e.g., the Earth and the Moon, each rotating in coplanar circular orbits about their mutual barycenter.¹¹ Further, it is assumed that the spacecraft and the primary bodies are all point masses. The motion of the spacecraft in the CR3BP framework is derived in the context of a dextral orthonormal triad \hat{x} , \hat{y} and \hat{z} that constitutes a coordinate system, \mathbb{R} , rotating at a fixed rate, consistent with the revolution of the primary bodies about their barycenter. The \hat{x} axis in the rotating frame is the line joining the primaries, i.e., the Earth-Moon line; the positive direction is a view from the Earth towards the Moon. The direction normal to the Earth-Moon orbit plane is denoted by the positive \hat{z} direction. Finally, \hat{y} completes the right-hand coordinate system. The three spacial directions are used to describe the nonlinear spacecraft motion. The position vector is represented as $\bar{r} = [x, y, z]^T$ and velocity states by $\bar{v} = [\dot{x}, \dot{y}, \dot{z}]^T$. Again, for convenience, the 6-dimensional state is written by $\bar{x} = [\bar{r}^T, \bar{v}^T]^T = [x, y, z, \dot{x}, \dot{y}, \dot{z}]^T$, where superscript 'T' implies transpose operation. Note that overbars represent vector quantities. The CR3BP dynamics facilitates understanding of the underlying nonlinear spacecraft motion rather than direct analysis in the higher-fidelity ephemeris model due to time-dependency as well as additional complexities. The model in the CR3BP also admits five equilibrium points, all in the xy plane, labelled as the libration points, or Lagrange points. Identified as L1 through L5, the first three L1, L2 and L3 are collinear and located on the line joining the primary bodies. In the Earth-Moon system, the equilibrium point L1 lies on the \hat{x} -axis between the Earth and the Moon, while L2 is on the far side of the Moon.

Periodic orbits in the CR3BP system are explored as long horizon baseline trajectories for various mission scenarios. The location, stability characteristics as well as the accessibility to these orbits determine the suitability of various orbits as potential mission candidates. Within the Earth-Moon system, a family of 3-dimensional periodic trajectories near the L1 and L2 equilibrium points, commonly termed as halo orbits, are explored as potential destinations for a long-term facility in cislunar space.¹² Specifically for the Gateway mission, an L2 southern halo orbit is the current focus. The family of the L1 and L2 southern halo orbits in the Earth-Moon system are plotted in Figure 1. Some members of the L1 and L2 halo family with close lunar passage and high out-of-plane amplitudes are stable or nearly stable based on a variational linear stability analysis.¹ The stability index, $\nu_i = (1/2)(\lambda_i + 1/\lambda_i)$, is a parameter defined to measure the stability characteristics for a periodic orbit, where λ_i are the eigenvalues from the monodromy matrix, i.e., the state transition matrix computed over precisely one orbital period. Figures 2(a) and 2(b) describes the evolution of the stability indices as a function of perilune radii for members of the L1 and L2 halo orbits, respectively. For stable orbits, the absolute value of stability index is less than or equal to one, i.e., $|\nu_i| \leq 1$. The Near Rectilinear Halo Orbits (NRHOs) are a subset of the halo orbit family that are stable or nearly stable orbits, as measured using stability index, the range of which is marked in Figure 2. Within Figure 1 the orbits colored in red are the NRHOs in both the L1 and the L2 families. Only the halo orbits that do not intersect the Moon's surface are plotted in the configuration space. For the stationkeeping analysis, orbits are selected with different perilune radii including those that demonstrate simple resonance ratios.

HIGHER-FIDELITY MODEL

The higher-fidelity ephemeris model relies on the N -body relative equations of motion to render a more accurate representation of the spacecraft motion, one that resembles the underlying dynamics predicted by the CR3BP model. Any analysis accomplished in the CR3BP model is ultimately validated in the higher-fidelity ephemeris model to ensure the appropriateness for the real problem. NASA's Jet Propulsion Laboratory (JPL) offers a package for numerical approximations of the time-varying relative locations of celestial bodies in terms of SPICE Kernels.¹³ The position and velocity states in the CR3BP model when propagated in the ephemeris model using SPICE data, deviates from the path predicted by the CR3BP model. A continuous natural trajectory in the higher-fidelity model is generated by stacking multiple revolutions of the CR3BP orbit and correcting for position and velocity continuity using a multiple shooting algorithm.¹⁴ The iterative process yields a quasi-periodic trajectory in the higher-fidelity ephemeris model that resembles the geometry of the corresponding orbit in the CR3BP, and serves as a virtual reference solution for stationkeeping operations. The entire virtual reference is updated over time as appropriate. To accommodate the updated reference, infrequent long horizon orbit correction maneuvers are easily incorporated as a part of the stationkeeping algorithm. The fidelity of the model is enhanced by adding the effect of a large number of celestial bodies in the N -body problem at the cost of an increase in computational time. Since additional orbit determination errors are incorporated in the stationkeeping algorithm, addition of too many celestial bodies is nontrivial. Based on prior investigations,¹⁵ the gravitational forces due to the Earth, the Moon and the Sun, as well as the Solar Radiation Pressure (SRP), are the most dominant forces acting on the Earth-Moon halo orbits in the L1 and L2 region, and sufficient for this analysis. Consistent with other stationkeeping literature, gravitational force due to Jupiter is also considered.^{2,6} Ephemeris data is integrated using the DE421 model.

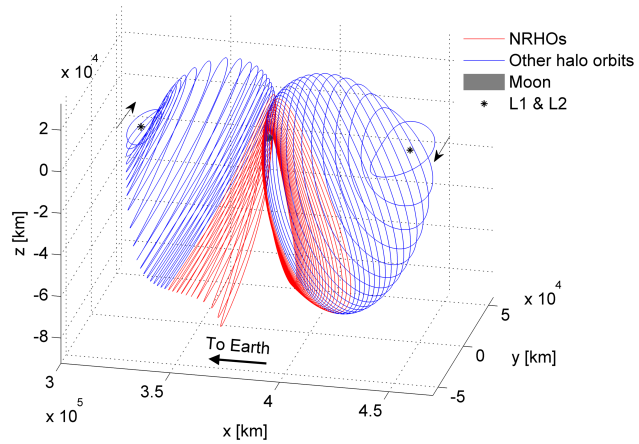


Figure 1: Earth-Moon L1 and L2 southern halo orbits

The iterative process yields a quasi-periodic trajectory in the higher-fidelity ephemeris model that resembles the geometry of the corresponding orbit in the CR3BP, and serves as a virtual reference solution for stationkeeping operations. The entire virtual reference is updated over time as appropriate. To accommodate the updated reference, infrequent long horizon orbit correction maneuvers are easily incorporated as a part of the stationkeeping algorithm. The fidelity of the model is enhanced by adding the effect of a large number of celestial bodies in the N -body problem at the cost of an increase in computational time. Since additional orbit determination errors are incorporated in the stationkeeping algorithm, addition of too many celestial bodies is nontrivial. Based on prior investigations,¹⁵ the gravitational forces due to the Earth, the Moon and the Sun, as well as the Solar Radiation Pressure (SRP), are the most dominant forces acting on the Earth-Moon halo orbits in the L1 and L2 region, and sufficient for this analysis. Consistent with other stationkeeping literature, gravitational force due to Jupiter is also considered.^{2,6} Ephemeris data is integrated using the DE421 model.

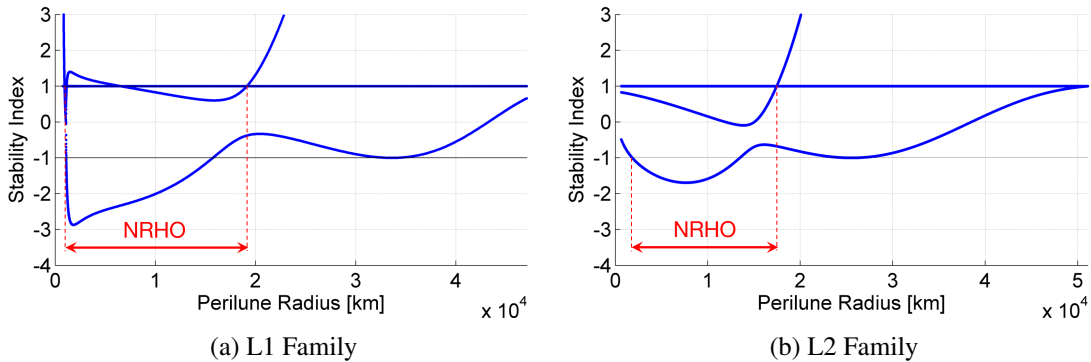


Figure 2: Stability index of different halo orbits in the Earth-Moon system

X-AXIS CROSSING CONTROL STATIONKEEPING STRATEGY

Any spacecraft is perturbed from the nominal path due to the sensitive dynamics along the orbit. Regular impulsive stationkeeping maneuvers are necessary for long-term sustainability of the spacecraft near the virtual reference orbit. Recent analyses have focused on the x -axis control algorithm to deliver maneuvers for successful cislunar missions^{9,16} and is currently employed for analysis on the Gateway mission.^{2,6,10,17} The x -axis control strategy generally relies on the symmetry of the halo orbits across the xz plane in the CR3BP framework. Additionally, the rotating \dot{x} value along the orbit at the xz plane crossing is zero in the CR3BP; the concept is exploited for orbit maintenance operations. The natural trajectory in the ephemeris model that resembles the NRHO does not necessarily possess a precise value of $\dot{x} = 0$ at the xz plane crossing, therefore, the rotating \dot{x} value that is targeted along the actual trajectory is not precisely zero. The stationkeeping algorithm constrains the correction process to target the actual \dot{x} value along a long horizon virtual reference path at the xz plane crossing within an acceptable tolerance.

In the stationkeeping process, the 6-dimensional spacecraft state is originally introduced at the halo orbit injection state along a long horizon virtual reference solution. An assumed Gaussian noise, of specified mean and variance, is incorporated in both position and velocity states. Solar radiation pressure is introduced with errors in the coefficient of reflectivity C_r and the cross-sectional surface area of the spacecraft model. The perturbed states are propagated downstream to a predetermined maneuver location, generally closer to the apoapsis region, and a maneuver $\Delta\bar{v}$ is calculated to meet the goal of achieving the \dot{x} value along the virtual baseline at a specified downstream xz plane crossing, within some predefined tolerance; 0.45 m/s in this investigation.² Maneuvers are generated by targeting the xz plane crossings at the specified target horizon time, near the periapsis region. To simulate for the limitations of the thrusters, maneuver execution errors are included with the computed maneuver, and implemented. Along the subsequent path, the states are updated and further perturbed with navigational errors and solar radiation pressure errors. The procedure is continued till the simulated epoch time exceeds the mission duration. The total sum of the maneuvers $|\Delta\bar{v}|$ over each run is recorded. Since white noise is generated randomly, a Monte Carlo simulation is performed over 100 runs with different seeds and the mean cost is estimated.¹⁴ It has been observed that with 100 samples, a sufficient level of precision is achieved while estimating the mean.^{5,18} The total cost is then linearly extrapolated over one year to estimate an annual maintenance cost. In certain cases, the virtual reference solution is updated incorporating infrequent long horizon orbit correction maneuvers; for consistency, the cost of which is not directly added to the annual stationkeeping cost estimate.

Orbit determination and model error

To simulate the perturbations that a spacecraft experiences, different error levels in the orbit determination process (injection error, navigational errors and maneuver execution errors) and modeling formulations are introduced. While simulating the stationkeeping process, the spacecraft states are intentionally perturbed from the virtual reference solutions. Two different navigation error levels are considered, a low orbit determination error (ODE) level with mean 0 and standard deviation (3σ) of 1 km in position magnitude and 1 cm/s in velocity magnitude, and a relatively high orbit determination error (ODE) level with mean 0 and standard deviation (3σ) of 10 km in position magnitude and 10 cm/s in velocity magnitude. The error levels at orbit insertion are consistent with the navigation error. Further, maneuver execution error is incorporated as a fixed magnitude of 0.03 cm/s in any arbitrary direction.

Solar radiation pressure (SRP) is incorporated in the model while propagating the spacecraft states, however, the exact orientation of the spacecraft is undetermined. Hence SRP errors are

introduced to simulate a perturbing acceleration. A cannonball model is assumed for the spacecraft with mass 25848 kg, projected area of 50 sq.m. and a perfectly reflective surface with coefficient of reflectivity $C_r = 2$.^{2,7} Uncertainty (1σ) in the projected area of 5% and uncertainty in C_r of 10% is assumed for all simulations.^{2,7}

Stationkeeping parameters

The annual orbit maintenance cost as well as the boundedness of the spacecraft motion near a virtual reference solution is influenced by various user-defined parameters considered within the stationkeeping algorithm. A stationkeeping technique that delivers impulsive orbit maintenance maneuvers using the x -axis control approach, is influenced by three factors, namely, coast duration, maneuver location and the target horizon time, as defined by Muralidharan and Howell.¹⁰ Coast duration is defined as the minimum time duration between two successive maneuvers. Maneuver location is the location along the orbit where the maneuver is implemented. For convenience, these locations are labelled in terms of osculating true anomaly as well as mean anomaly. Finally, target horizon, or target horizon time, is defined as the length of time between the maneuver location and the specified target location, that is the xz plane crossing near the periapsis region. The target horizon is labelled in terms of the number of revolutions downstream, along the orbit, from the maneuver location. The mutual interaction between the parameters, i.e., coast duration, maneuver location and target horizon, is demonstrated in the flowchart in Figure 3. The maneuver characteristics are determined by the interaction between the flow evolving from one maneuver location to the following along the coast arc, and the flow evolution from the maneuver location to the target.

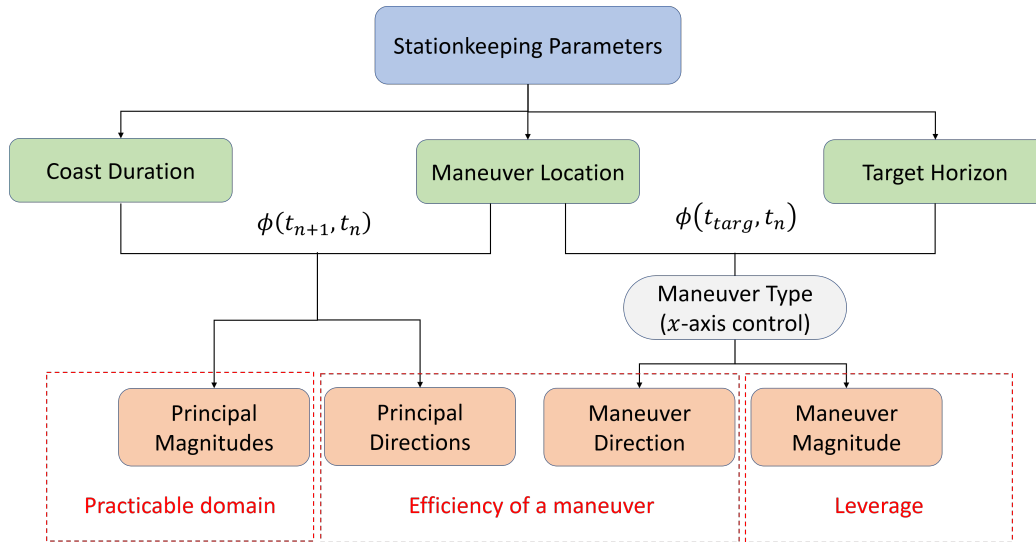


Figure 3: Stationkeeping parameter efficiency flowchart.¹⁰

Effect of maneuver location and coast duration The spacecraft advances along a ballistic trajectory between two successive impulsive maneuver locations, for a time interval specified by the coast duration. For small perturbations consistent with orbit determination prevalent in the stationkeeping process as well as the magnitude of stationkeeping maneuvers, a linear state transition matrix (STM) is generally reliable to assess the impact of deviations on the states at some time downstream, where the subsequent maneuver is executed. The linear flow between two successive maneuvers locations is visualized using the Cauchy-Green tensor (CGT), a function of the STM, that decomposes the flow into different mutually orthogonal directions, along which components of

perturbations grow independent of the other. The Cauchy-Green tensor (CGT), or simply ‘C’, is a product of the transpose (superscript T) of the state transition matrix (STM) defined as

$$\mathbb{C}(t_f, t_0) = \phi(t_f, t_0)^T \phi(t_f, t_0) \quad (1)$$

that renders the square of the magnitude of the final deformation to the initial deformation such that

$$\|\delta \bar{\mathbf{x}}_f\|^2 = \delta \bar{\mathbf{x}}_f^T \delta \bar{\mathbf{x}}_f = \delta \bar{\mathbf{x}}_0^T \phi(t_f, t_0)^T \phi(t_f, t_0) \delta \bar{\mathbf{x}}_0 = \delta \bar{\mathbf{x}}_0^T \mathbb{C}(t_f, t_0) \delta \bar{\mathbf{x}}_0. \quad (2)$$

where t_0 and t_f are the initial and final epochs while $\phi(t, t_0) = \frac{\partial \bar{\mathbf{x}}(t)}{\partial \bar{\mathbf{x}}_0}$ is the linear STM.^{19,20} The STM is evaluated on a reference trajectory, $\bar{\mathbf{x}}^*(t)$, to map the initial perturbed states, $\delta \bar{\mathbf{x}}_0$, to the final perturbed isochronous states, $\delta \bar{\mathbf{x}}_f$. The eigen-decomposition of the CGT, or the singular value decomposition of the STM, offers information about directions and magnitudes of the perturbation growth. The eigen-decomposition of the CGT yields the eigenvalues λ_i and the eigenvectors \mathbb{V}_i , such that the contraction or expansion of the local phase space is represented by σ_i in the directions along \mathbb{V}_i . Here, $\sigma_i = \sqrt{\lambda_i}$. The singular value decomposition (SVD) of the STM,

$$\mathbb{U} \Sigma \mathbb{V}^* = \phi(t_f, t_0) \quad (3)$$

offers additional directional information, \mathbb{U} , also $\mathbb{U} = \phi(t_f, t_0) \mathbb{V}$. The columns of matrix \mathbb{U} yield the stretching directions at the final epoch. For a square matrix, ϕ , Σ is a diagonal matrix with $\sigma_1 > \sigma_2 > \dots > \sigma_n$, such that $\sigma_i = \Sigma_{ii}$, is the element in Σ in the i^{th} row and i^{th} column. The principal stretching directions at the initial time, along the propagated arc, is capture by matrix \mathbb{V} . The matrices \mathbb{U} and \mathbb{V} are each orthonormal. Figure 4 illustrates the contraction and expansion along different flow directions using the example of a two-dimensional system transformed through CGT.

Maneuver locations and coast durations are variables, thus, their precise values are measured in terms of mean anomaly and osculating true anomaly, as described by Muralidharan and Howell.¹⁰ Since the NRHO is a periodic orbit in the CR3BP, the mean anomaly, θ_{MA} , is defined as $\theta_{MA} = 2\pi t/T \text{ rad} = 360 t/T \text{ deg}$, where T is the time period for the NRHO while t is the time of propagation beyond the most recent periapsis as described in the circular restricted three-body problem. Since the NRHO is a non-Keplerian orbit, an osculating true anomaly, θ_{TA} , is simply a representative angle as viewed in the rotating frame, defined with respect to Moon as the central body.²¹

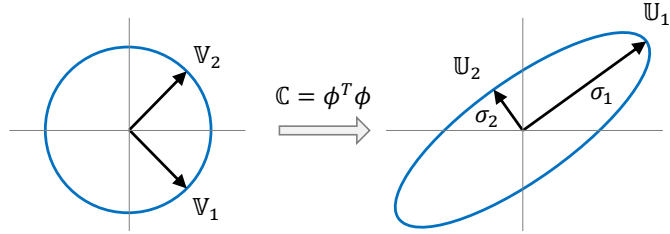


Figure 4: Principal stretching directions.

Different elements of the STM offer correlation between a corresponding initial state to a final state. The flow between two successive impulsive maneuvers, at time t_0 and t_f respectively, is delivered by the STM evaluated along a ballistic segment, i.e., φ_C , such that

$$\varphi_C(t_f, t_0) = \begin{bmatrix} \varphi_{C,r,r} & \varphi_{C,r,v} \\ \varphi_{C,v,r} & \varphi_{C,v,v} \end{bmatrix} = \begin{bmatrix} \frac{\partial \bar{r}_f}{\partial \bar{r}_0} & \frac{\partial \bar{r}_f}{\partial \bar{v}_0} \\ \frac{\partial \bar{v}_f}{\partial \bar{r}_0} & \frac{\partial \bar{v}_f}{\partial \bar{v}_0} \end{bmatrix} \quad (4)$$

where $\varphi_{C,r,r}$, $\varphi_{C,r,v}$, $\varphi_{C,v,r}$ and $\varphi_{C,v,v}$ are the 3×3 submatrices of 6×6 matrix φ_C . Any n^{th} and

$(n + 1)^{\text{th}}$ maneuver at time t_n and t_{n+1} respectively, without loss of generality, is synonymous to $t_n = t_0$, the initial time at which the maneuver is implemented, and $t_{n+1} = t_f$, the final time along the propagated segment. Therefore, $\varphi_C(t_f, t_0) = \phi(t_{n+1}, t_n)$. One of the most useful requirements of a stationkeeping algorithm is to minimize the propellant cost; then the assessment of successive maneuver magnitudes is the primary concern. Therefore, the 3×3 dimensional submatrix, $\varphi_{C,v,v}$, that maps the initial velocity perturbation, $\delta\bar{v}_0$, to the final velocity change, $\delta\bar{v}_f$, offers more relevant characteristics. Further, as illustrated by Muralidharan and Howell,¹⁰ the dynamics in the halo orbit region are more sensitive to velocity perturbations than the position perturbations, therefore, the flow described by the $\varphi_{C,v,v}$ submatrix generally suffices to identify sensitive regions along the orbit. Also, the trajectory segments that originate or terminate near the periapsis regions are more sensitive to perturbations, therefore, maneuvers in such regions are generally avoided.

Effect of maneuver location and target horizon For an x -axis control strategy, the rotating \dot{x} value is targeted across different xz plane crossings near the periapsis region. The flow between the maneuver location and the target location, as defined by the state transition matrix, $\varphi_T = \phi(t_{\text{Target}}, t_0)$, determines the maneuver characteristics, where the time difference between t_0 and t_{Target} is labelled as the target horizon time. The stationkeeping control effort is represented by

$$\Delta\dot{x}_f = [\varphi_{T,44} \quad \varphi_{T,45} \quad \varphi_{T,46}] \Delta\bar{v}_0 \quad (5)$$

where, $\Delta\dot{x}_f$ is the change desired in the rotational \dot{x} value at the target xz plane crossing, and $\Delta\bar{v}_0 = [\Delta\dot{x}_0, \Delta\dot{y}_0, \Delta\dot{z}_0]^T$ constitutes a column vector that is comprised of three scalar independent control variables that comprise the impulsive maneuver. Lastly, $[\varphi_{T,44} \quad \varphi_{T,45} \quad \varphi_{T,46}]$ is the relevant submatrix of the STM, φ_T . The subscripts, i and j , in $\varphi_{T,ij}$, indicate the element in the i^{th} row and j^{th} column. For convenience, define $\bar{M} = [\varphi_{T,44} \quad \varphi_{T,45} \quad \varphi_{T,46}]^T$ as a 3×1 column vector and, henceforth, $\Delta\dot{x}_f = \bar{M}^T \Delta\bar{v}_0$. One of the goals of a stationkeeping process is reducing the propellant costs, hence, a minimum norm solution that delivers the smallest maneuver magnitude is generally an appropriate choice. Since the control equation $\Delta\dot{x}_f = \bar{M}^T \Delta\bar{v}_0$ is equivalent to the dot product between \bar{M} and the $\Delta\bar{v}_0$ vector, the maneuver magnitude is deduced as

$$|\Delta\dot{x}_f| = |\bar{M}| |\Delta\bar{v}_0| \cos\vartheta \quad \longrightarrow \quad |\Delta\bar{v}_0| = \frac{|\Delta\dot{x}_f|}{|\bar{M}| \cos\vartheta} \quad (6)$$

where $\cos\vartheta$ is the angle between vectors \bar{M} and $\Delta\bar{v}_0$. The smallest maneuver $|\Delta\bar{v}_0|$ is delivered for $\cos\vartheta = 1$, or, $\vartheta = 0^\circ$, i.e., the $\Delta\bar{v}_0$ vector is aligned in the direction of \bar{M} . As a result, a minimum norm solution for stationkeeping produces a maneuver magnitude of

$$|\Delta\bar{v}_0|_{\text{min-norm}} = \frac{|\Delta\dot{x}_f|}{|\bar{M}|} \quad (7)$$

along the direction of \bar{M} . In contrast to the maneuver direction, the maneuver magnitude actively depends on the change desired in rotational velocity, $\Delta\dot{x}_f$. Of course, the scalar $\Delta\dot{x}_f$ one that evolves with time, thus, the ratio of maneuver magnitude to the magnitude of the initial perturbation is a more reliable metric, i.e.,

$$|\Delta\bar{v}_0|_{\text{min-norm}} = \frac{|\bar{B}^T \Delta\bar{x}_0|}{|\bar{M}|} \leq \frac{|\bar{B}^T| |\Delta\bar{x}_0|}{|\bar{M}|} \quad \longrightarrow \quad \frac{|\Delta\bar{v}_0|_{\text{min-norm}}}{|\Delta\bar{x}_0|} \leq \frac{|\bar{B}|}{|\bar{M}|} \quad (8)$$

where $\Delta\dot{x}_f = \bar{B}^T \Delta\bar{x}_0$ with $\bar{B} = [\varphi_{T,41} \quad \varphi_{T,42} \quad \varphi_{T,43} \quad \varphi_{T,44} \quad \varphi_{T,45} \quad \varphi_{T,46}]^T$ as the submatrix of φ_T that correlates the initial state perturbation that delivers a final \dot{x} change, in a linear sense. The vector

$\Delta\bar{\mathbf{x}}_0 = [\Delta x_0, \Delta y_0, \Delta z_0, \Delta \dot{x}_0, \Delta \dot{y}_0, \Delta \dot{z}_0]^T$ is the initial perturbed state. The ratio $\frac{|\hat{B}|}{|\hat{M}|}$ offers an upper limit on the maneuver magnitude that is required to overcome a unit initial perturbation. Generally, a low value of $\frac{|\hat{B}|}{|\hat{M}|}$ implies that a smaller maneuver magnitude is required to overcome a unit initial perturbation, hence, suitable for maneuver placement and/or implementation.

The direction of the maneuver, \hat{M} , is a vital parameter that assists in evaluating the efficiency of a potential maneuver in maintaining the spacecraft in the vicinity of a virtual reference solution. The stretching directions for the matrix, φ_C , are available; such a quantity offers insight for predicting a variation that likely overcomes the spacecraft deviate from the virtual reference path. In configuration space, if the maneuver direction, \hat{M} , is aligned in the maximum stretching direction \mathbb{V}_1 , along which $\sigma_1 > 1$, then the implemented maneuver causes the maximum change in the magnitude of the state at the following maneuver location, henceforth, growing the spacecraft deviation from the nominal path. In contrast, if the maneuver direction, \hat{M} , is aligned perpendicular to the maximum stretching direction \mathbb{V}_1 , then the executed maneuver delivers less variation of the state away from the nominal path. If the stretching magnitudes along the directions associated with σ_2 and σ_3 are less than a nondimensional value of 1, then the plane represented by the $\mathbb{V}_2 - \mathbb{V}_3$ vectors defines a restoring plane. If, only $\sigma_3 < 1$, then the direction along the \mathbb{V}_3 vector is a restoring direction. The restoring plane or the restoring direction is decisive as the magnitude of variations at the end of the propagated arc diminish in comparison to any perturbations at the beginning. The maneuvers, when executed in the restoring plane or along the restoring direction, decreases the spacecraft deviation at the downstream locations, thereby maintaining the spacecraft boundedness. Regions such that the maneuver and the most stretching direction are almost perpendicular facilitate efficient maneuvers. Again, maneuvers perpendicular to the maximum stretching direction do not always imply that they are aligned in a restoring subspace, rather the alignment depends on the values of σ_2 and σ_3 . Any component of the maneuver aligned in a stretching direction grows over time, depending on the stretching magnitude in that direction. A long horizon orbit corrections maneuver is delivered when the growth of the deviation is significantly large such that the routine short horizon stationkeeping maneuvers are incapable of overcoming the errors.

Low Perilune Radius Near Rectilinear Halo Orbits

Davis et al.⁶ as well as Guzzetti et al.² have demonstrated stationkeeping for Earth-Moon L2 NRHOs, by implementing maneuvers once per revolution, generally at (or near) the apoapsis. The annual orbit maintenance costs estimated by targeting the rotating x -velocity value at the xz plane crossing 6.5 revolutions downstream are relatively low, for various orbit determination error levels. In the conventional approach, since maneuvers are implemented only once per revolution, at the apoapsis, the effect of an implemented maneuver at one apoapsis is substantial when propagated to the following apoapsis. Any component of the maneuver along the largest stretching direction is amplified over the propagated arc causing a larger deviation when it reaches the subsequent apoapsis and the phenomenon continues till the deviation is sufficiently large and the spacecraft may be escaping. For the L2 NRHOs, orbits with perilune radius between 2000-9000 km and with one maneuver per orbit, executed at the apoapsis, i.e., maneuver location at $\theta_{MA} = 180^\circ$ and a coast arc of 360° (1 time period), there exists one stretching direction and two non-stretching directions forming a restoring plane as demonstrated by Muralidharan and Howell,¹⁰ thereby, ensuring maneuvers are perpendicular to the stretching direction and establishing the stability of the maneuvers. Figure 5(a) describes the dimensions of the stretching subspaces for the L2 NRHO with 3200 km perilune radius that is the current baseline for the Gateway mission. Again, as indicated for the combination of maneuver location at $\theta_{MA} = 180^\circ$ and coast arc of 360° there is one stretching and two non-stretching subspaces. The angle between the direction of the maneuver \hat{M} and the most stretching direction of

$\varphi_{C,v,v}$ varies for different target horizons. For the L2 NRHOs, a targeting horizon located 1.5 revs ahead generates a significant angle between the maneuver and the most stretching direction, while for the 6.5 rev target horizon the angle is closer to 90 degrees as illustrated in Figure 6. For the range of NRHOs under investigation, targeting 1.5 rev horizon is not recommended, as maneuvers possess a significant component in the maximum stretching direction; the deviation size and the maneuver size continuously increase with time and, eventually, diverge from the virtual reference trajectory. In contrast, for target horizons where the maneuver direction is almost perpendicular to the most stretching direction, i.e., aligned with the restoring plane, state variations at the initial time do not induce a large final variation, hence, the spacecraft remains bounded near the virtual reference trajectory. Depending on the NRHO of interest, selecting 6.5 rev, 4.5 rev and 2.5 rev target horizons offer improved performance. Targeting beyond 6.5 rev horizon is computationally intensive and does not necessarily yield any significant improvements in orbit maintenance costs. For different L2 NRHOs, the annual stationkeeping costs are listed for both low (3σ : 1 km and 1 cm/s) and high (3σ : 10 km and 10 cm/s) orbit determination error levels in Table 1.

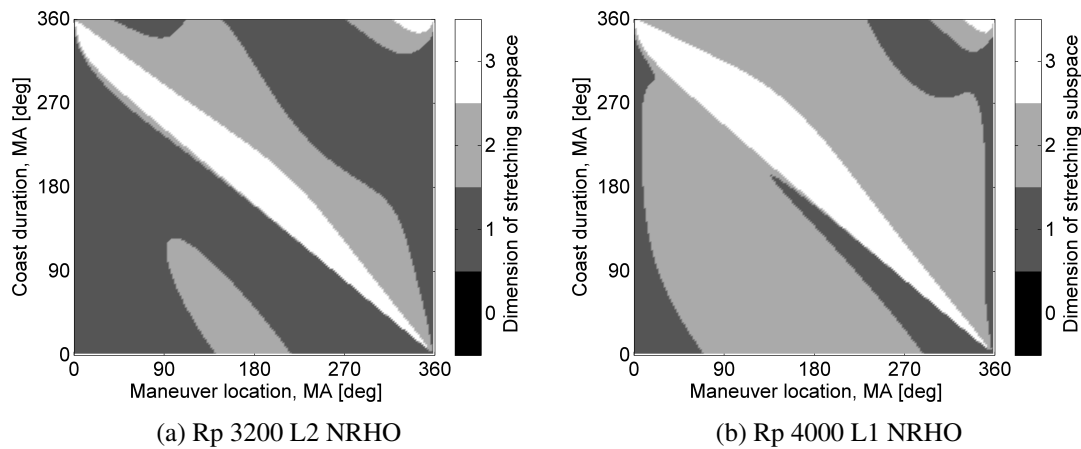


Figure 5: Number of stretching subspace for different combination of maneuver location and coast duration measured in Mean Anomaly

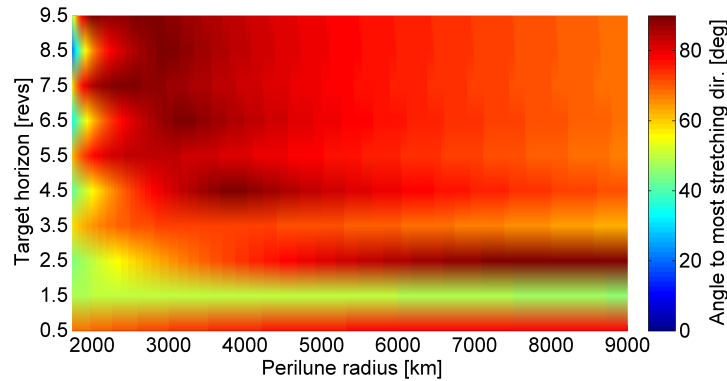


Figure 6: Angle between the estimated maneuver and the most stretching direction

Near rectilinear halo orbits in the L1 region are also potential candidates for space exploration missions. Although the NRHOs in the L1 region demonstrate similar stability characteristics to the L2 NRHOs, as defined by eigenvalues of the linear variational flow, they do not mirror all the

Table 1: Annual stationkeeping cost [m/s] along L2 NRHOs with target horizon of 6.5 revs.

Perilune radius [km]	3200	4000	4800	5645	6400	7200
Low ODE (3σ : 1 km & 1 cm/s)	0.16	0.15	0.15	0.15	0.16	0.15
High ODE (3σ : 10 km & 10 cm/s)	0.91	0.91	0.82	0.86	0.83	0.78

properties as that of L2 NRHOs. In the L2 NRHOs, as perilune radius decreases the apolune radius also decreases, however, L1 orbits do not possess similar characteristics, rather, as perilune radius of L1 NRHOs decrease, the apolune radius initially decreases and then increases rapidly, forming high out-of-plane amplitudes. Stationkeeping maneuvers maintain spacecraft in the neighborhood of a virtual reference solution depends on the maneuver locations and the target horizon time, rather than the stability index in general. The interaction between the flow evolving between one maneuver to the other as well as the flow evolution from maneuver location to target are different across the NRHOs in the L1 family in comparison to the L2 family. Observations and results obtained for L2 NRHOs cannot be generalized for the L1 family.

A Cauchy-Green tensor assists in visualizing the flow of the magnitude of the state vectors in the neighborhood of a virtual reference trajectory by again decomposing into different stretching directions that are orthogonal to each other, such that the flow along each of the decomposed directions evolves independent of the other. The number of directions with a magnitude of stretching, $\sigma_i > 1$, is labelled as the stretching subspace. For a 3-dimensional flow, the number of stretching subspace varies between 0 and 3. A 0-dimensional stretching subspace is characteristics of regions where the magnitude of perturbation always diminishes along a propagated arc, irrespective of the direction of maneuver. If the dimensions of stretching subspace is 1, there exists a single direction along which perturbations grow while a restoring plane exists where perturbations diminish downstream. Similarly, a 2-dimensional stretching subspace indicates a plane along which perturbations expand and then one restoring direction. Finally, all directions in a 3-dimensional stretching subspace amplify perturbations, certainly causing a larger variations downstream. Any maneuvers in a region with a 3-dimensional stretching subspace must be avoided as they are malignant. Figures 5(a) and 5(b) are maps that correspond to the dimension of stretching subspace for flow originating and terminating at different locations along the orbit, computed for a perilune radius 3200 km (L2 NRHO) and a perilune radius 4000 km (L1 NRHO), respectively. The characteristics of the other L1 and L2 NRHOs are similar to the members plotted in Figure 5. Clearly, there is a distinct difference in the number of stretching subspaces over different maneuver locations, described in terms of mean anomaly, for the L1 NRHO as compared to L2 NRHO. These subtle differences cause variations in the stationkeeping performance between the L1 NRHO family versus the L2 NRHO family.

Symmetric one maneuver per orbit Implementing one maneuver per orbit on an axis of symmetry for stationkeeping is equivalent to delivering one maneuver per orbit at 180° mean anomaly or 180° osculating true anomaly once per revolution, i.e., at apoapsis location every revolution. From the map in Figure 5, there exists only a 1-dimensional stretching subspace for an L2 NRHO with perilune radius 3200 km, corresponding to maneuver at 180° mean anomaly and a coast duration of 360° . Hence, a maneuver away from the most stretching direction is likely to offer long-term stability. Other low perilune L2 NRHOs also possess similar characteristics. The magnitudes of stretching, σ_i , along different L1 NRHOs, appear in Figure 7 for flow between two successive apoapses. In contrast to the L2 NRHOs with a 1-dimensional subspace for flow between two successive apoapsis, there exists a 2-dimensional stretching subspace for L1 NRHOs with low perilune radii. Therefore, ensuring a maneuver away from the most stretching direction is not sufficient for long-term stability. A maneuver is effective if it is perfectly aligned in the restoring direction, i.e.,

mutually perpendicular to both the most stretching and the intermediate stretching direction. However, targeting the xz plane crossing near the periapsis regions does not deliver maneuvers precisely along the restoring direction. Further, if the magnitude of stretching in the intermediate stretching direction is not significantly larger than 1, maneuvers perpendicular to the most stretching direction is still unlikely to maintain the spacecraft near the virtual reference solution for a long time as variations increase gradually over time. Perhaps, maintaining spacecraft for a shorter duration may still be possible. Nevertheless, as seen in Figure 7, for L1 NRHOs with magnitude of $\sigma_2 > 1$, which is significant, any component of maneuvers along the intermediate stretching direction amplifies over time substantially, causing divergence from the baseline trajectory. A symmetric single maneuver per orbit implemented at the apoapsis is not generally an efficient choice for the L1 NRHOs.

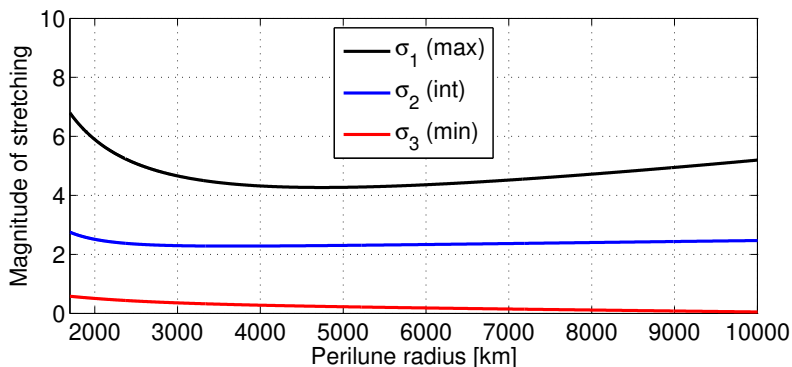


Figure 7: Magnitude of stretching σ_i along different \mathbb{U}_i direction for various L1 NRHOs.

Symmetric two-maneuvers per orbit A single symmetric maneuver executed at the apoapsis on an L1 NRHO may not be efficient, however, implementing two maneuvers per orbit approximately symmetric about the apoapsis, offers more possibilities. Figure 8 corresponds to the map of several combinations of maneuver location and coast duration, as well as the associated angle from the most stretching direction, for the L1 NRHO with perilune radius 4000 km described in terms of osculating true anomaly. The map is generated by targeting the 1st xz plane crossing near the periapsis. Of course, several combinations may exist, but an effective strategy introduces both maneuvers, or at least one with an almost 90° angle between the most stretching direction and the maneuver direction. One such combination is denoted with white dots in Figure 8. In this case, symmetric maneuvers are selected at 150° and 210° true anomaly values, that corresponds to the x -coordinate of the white dots. The y -coordinate of each of the white dots corresponds to the coast duration till the subsequent maneuver location. For visual simplicity, the angle swept by the spacecraft along the orbit as a result of the selected maneuvers are represented in terms of white dotted lines. The maneuver at 210° is aligned almost perpendicularly to the most stretching direction, and offers an appropriate choice. Since maneuvers are symmetric about apoapsis in this case, the maneuver

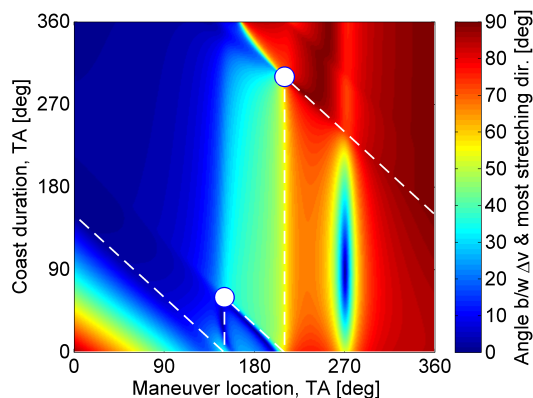


Figure 8: Symmetric two-maneuvers per orbit combination for an L1 NRHO with 4000 km perilune radius. Target: 1st xz plane crossing near periapsis. Maneuver location: 150° , 210° TA.

location at 150° true anomaly (TA) is complementary and there are no degrees of freedom for its selection. The maneuver at 150° TA possess a significant component in the stretching directions but since the propagated trajectory traverses through the apoapsis region, the resulting instability is limited. The short horizon maneuvers generated at 150° and 210° are a plausible combination. Since maneuvers may include a component in the intermediate stretching direction with a stretching magnitude marginally greater than 1, perturbations do grow, but at a very low rate. Some long-term simulations result in trajectories deviating away from the virtual reference solution as the corrective stationkeeping maneuvers with a component in the intermediate stretching direction along which variations amplify; an occasional long horizon maneuver overcomes such predictable trends. Application to different NRHOs and different target horizons yield different maps, for which feasible solutions employing a strategy for symmetric two-maneuver per orbit may or may not exist, hence cannot be generalized.

Symmetric three-maneuvers per orbit A scheme using symmetric three-maneuvers per orbit is an extended version of the symmetric two-maneuvers per orbit approach. Due to symmetry, one of the maneuvers is executed at the apoapsis, therefore, effectively equivalent to selecting a symmetric two-maneuver combination, with an additional maneuver at the apoapsis. Figures 9 corresponds to a three-maneuver combination noting the maneuver locations and coast duration, as well as the associated angle described in terms of osculating true anomaly from the most stretching direction, for the L1 NRHO with perilune radius 4000 km. The map is generated by targeting the 1st xz plane crossing near the periapsis. In comparison to the symmetric two-maneuver per orbit case in Figure 8, the time duration for propagation after the maneuver at 150° is essentially halved to accommodate a maneuver at the apoapsis. A three-maneuver combination decreases the time of propagation after the maneuver at 150° TA to the subsequent maneuver at 180° TA. The reduction in the time post maneuver, one that has a significant component in the stretching direction, comes as a trade-off of an added maneuver at 180° TA. Again, feasibility cannot be generalized as the maps are a reflective of a particular NRHO.

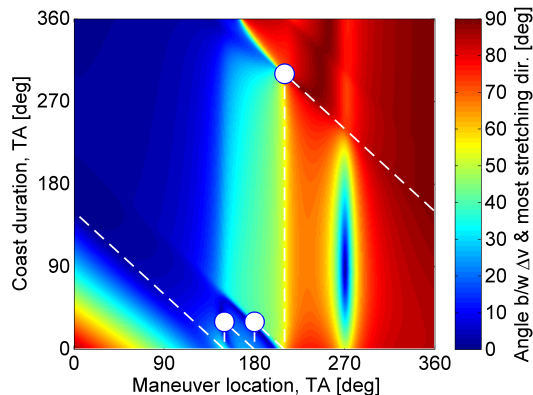


Figure 9: Symmetric three-maneuvers per orbit combination for an L1 NRHO with 4000 km perilune radius. Target: 1st xz plane crossing near periapsis. Maneuver location: 150° , 180° , 210° TA.

The number of maneuvers per orbit is a design choice and hence, more than three maneuvers per orbit is an option. As noted previously, several combinations of maneuver locations is straightforwardly generated through different maps for different halo orbits and different target horizon times. Some maps offer feasible combinations for a greater number of maneuvers per orbit. Nevertheless, too many maneuvers along a nearly stable NRHO may be redundant. The strategy as discussed is applicable for cases with higher number of maneuvers per orbit, but they are not explored here.

Asymmetric one maneuver per orbit Asymmetric maneuver combinations offers a larger domain for feasible solutions than the symmetric counterpart, due to more flexibility in exploring regions of the map. If only one maneuver per orbit is implemented, the coast duration must be 360° , repeating the location in configuration space every revolution, hence, the region to explore on the map is restricted to a line along the y -coordinate for 360° coast duration. It is then appropriate

to identify a maneuver location where a maneuver is aligned perpendicular to the most stretching direction. For example, Figure 10 corresponds to an asymmetric single maneuver location for the L1 NRHO with perilune radius 8000 km described in terms of osculating true anomaly. The map is generated by targeting the 2nd xz plane crossing near the periapsis. In this case, at 150° TA, a maneuver is aligned perpendicular to the most stretching direction, hence, offering a reasonable maneuver location. Again, maps are a reflective of the NRHO and the target horizon time; as a result, they may or may not offer any feasible regions for single maneuver per orbit cases.

Asymmetric two maneuvers per orbit A

larger degree of freedom exists in selecting asymmetric maneuver locations on an NRHO, that likely results in effective maneuvers. The maneuver locations are complementary to each other, i.e., the sum of their coast durations must add to 360°, for maneuvers that are expected to repeat every revolution. With higher flexibility, multiple combinations of maneuver locations are possible on the same map. Figures 11(a), 11(b) and 11(c) correspond to three different examples of asymmetric two-maneuver locations for the L1 NRHO with perilune radius 8000 km as described in terms of osculating true anomaly. The map is generated by targeting the 2nd xz plane crossing near the periapsis. Figure 11(a) offers plausible maneuver locations at 142° and 180° in true anomaly values, while Figure 11(b) introduces maneuver locations at 133° and 201° true anomalies, and finally, Figure 11(c) reciprocates maneuver locations at 139° and 194° true anomalies. These are only three distinct cases that are selected from the map, however, many such combinations are possible. Once again, despite larger flexibility in selection of the maneuver locations, feasibility of maneuver combinations depend on each individual maps that are generated for an NRHO and a target horizon time, and cannot be generalized.

The maneuvers generated by targeting the rotational \dot{x} value at certain xz -plane crossing downstream may have components along each of the principal stretching directions. The maneuver locations are selected based on the concept that a maneuver away from the most stretching direction is likely to result in the least magnitude of variation along the propagated trajectory downstream, based on linear variational analysis. In some cases, corrective stationkeeping maneuvers may still include a component in the intermediate stretching direction with a stretching magnitude greater than 1, along which the perturbations amplify. Depending on the rate of growth of the variations in the intermediate stretching direction, some trajectories deviate away from the virtual reference solution; an occasional long horizon maneuver overcomes such challenges. Stationkeeping costs estimated annually in this investigation, are only based on short horizon stationkeeping maneuvers that overcome orbit determination errors and unmodeled dynamics and do not include long horizon maneuvers, as they are specific to mission scenarios. Table 2 lists the estimated annual short horizon stationkeeping costs for various NRHOs, for different maneuver locations, coast durations and target horizon time. The values are estimated by propagating a trajectory for duration of 180 days. In practice, however, for a particular mission of interest, the overall cost of maintenance is the sum total of all short horizon and long horizon orbit maintenance maneuvers.²

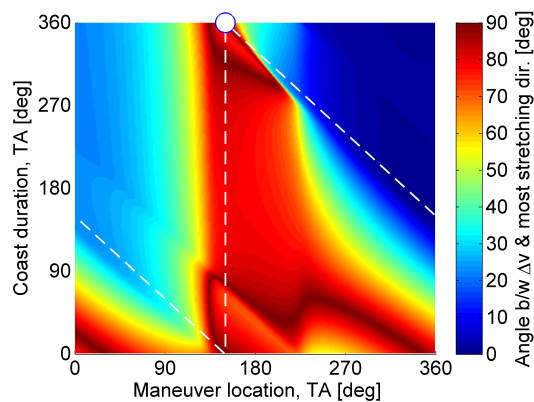


Figure 10: Asymmetric one-maneuver per orbit combination for an L1 NRHO with 8000 km perilune radius. Target: 2nd xz plane crossing near periapsis. Maneuver location: 150° TA.

Transition halo orbits

Transition halo orbits are members of the halo orbits in the L1 and L2 region, loosely identified with perilune radius between 10000 km to 22000 km, that when transitioned from CR3BP to higher-fidelity ephemeris model exhibits large variation in apse angles.⁶ An apse angle is described as the shift in the periapsis or the apoapsis of the orbit in the higher-fidelity model in comparison to the orbit in the CR3BP.¹ The range of orbits that exhibit large variation in apse angles typically exists as the transition occurs from stable NRHOs with relatively low perilune radius to the unstable members of the halo orbit family with relatively larger perilune radius. Some of the transition halo orbit members exhibit a simple resonance with the Earth-Moon sidereal and synodic periods. In the L2 family, the NRHO with an approximately 15000 km perilune radius is labelled as the 3:1 synodic resonant orbit, i.e., three time periods of the orbit corresponds to one synodic time period of the Moon around the Earth. Figure 12 illustrates the L2 NRHO with a 15000 km perilune radius transitioned from the CR3BP to ephemeris model on different starting epoch dates in the month of May in 2023. Clearly, the natural trajectories corresponding to each epoch exhibit different geometry in configuration space, indicating the sensitivity of the orbit states on epoch time. In particular, for the 3:1 synodic orbit, some similarity in geometry appears in 9-10 days intervals that roughly correspond to the time per revolution along the orbit in the CR3BP system.²² Other transition orbits in the L1 and L2 family display similar characteristics. Clearly, alternative strategies are possible to transition such orbits. But, to assess stationkeeping challenges, assume sample ephemeris trajectories such as those in Figure 12. As a result of such sensitivity, stationkeeping along these transition halo orbits is challenging and requires necessary modifications to the conventional impulsive stationkeeping algorithm.

The generation of a natural trajectory in the higher-fidelity ephemeris model is done in a consistent manner, considering the sensitivity

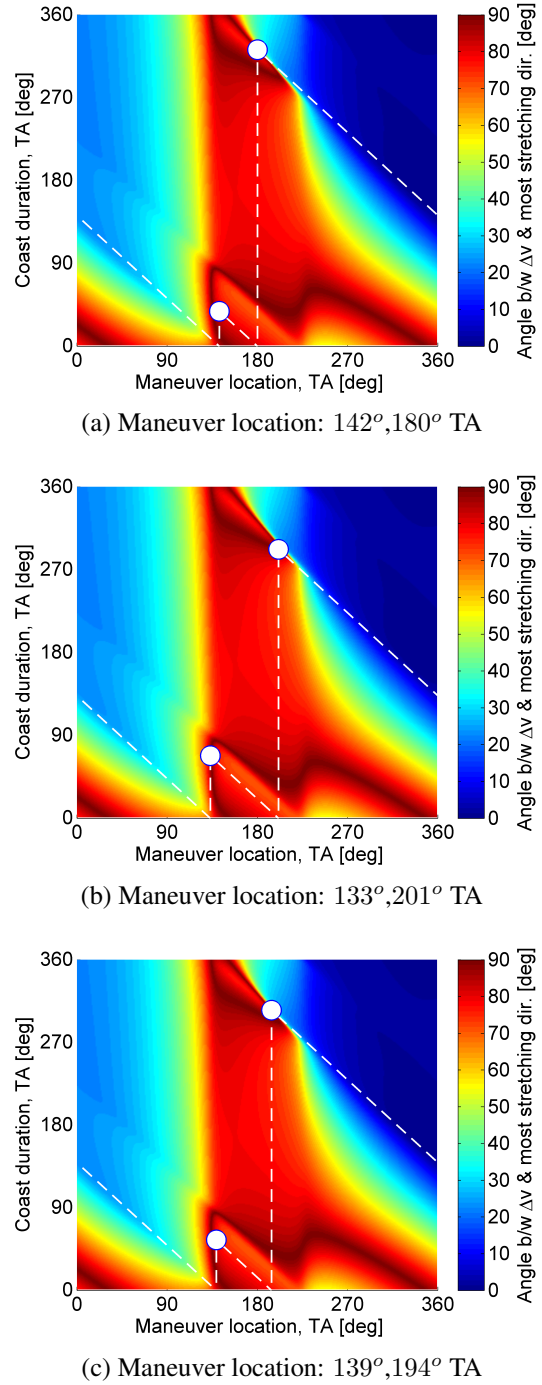


Figure 11: Asymmetric two-maneuvers per orbit combinations for an L1 NRHO with 8000 km perilune radius. Target: 2nd xz plane crossing near periapsis.

Table 2: Annual stationkeeping cost [m/s] along L1 NHROs

Perilune Radius [km]	Target xz -plane crossing #	Sym/Asym	# $\Delta\bar{v}$ /rev	Maneuver locations [TA]	Annual cost [m/s]	
					Low ODE	High ODE
4000	1	Sym	2	150, 210	2.21	6.25
4000	1	Sym	3	150, 180, 210	1.19	7.79
4000	3	Asym	1	188	0.74	1.61
5000	1	Sym	2	145, 215	2.47	5.46
5000	1	Sym	3	145, 180, 215	1.18	6.83
5000	1	Sym	2	150, 210	1.88	6.30
5000	1	Sym	3	150, 180, 210	1.21	7.73
5000	2	Asym	1	164	0.46	2.11
5000	5	Sym	1	180	0.20	0.72
6000	1	Sym	2	145, 215	2.31	6.47
6000	1	Sym	3	145, 180, 215	1.11	7.63
6000	2	Asym	1	160	0.52	2.24
7000	2	Asym	1	156	0.56	1.91
7000	5	Asym	1	171	0.20	0.78
8000	2	Asym	1	150	0.65	1.86
8000	2	Asym	2	142, 180	0.40	2.89
8000	2	Asym	2	133, 201	0.46	2.92
8000	2	Asym	2	139, 194	0.41	2.85

of the CR3BP states to the epoch time for transition halo orbits. A periodic orbit in the CR3BP is subdivided into 10 segments, equally spaced in time. The beginning node of each trajectory segment serves as a patch point for the multiple shooting process. To generate a natural trajectory approximately 12 time-periods in length, 12 revolutions of the orbit in the CR3BP are selected, and 'stacked' on top of each other, yielding a total of 121 patch points that serve as the initial conditions for the multiple shooting process. For consistency, the first patch point is selected at the apoapsis in the CR3BP model. Further, it is constrained that the location of first patch point is in the xz -plane. Through a Newton-Raphson iterative process, as demonstrated in literature, a natural trajectory is constructed that is continuous in position and velocity states, as well as in time.¹⁴ Of course, the geometry of the natural trajectory varies with the epoch date of the first patch point, a case for the L2 NRHO with 15000 km is demonstrated in Figure 12. The length of the natural trajectory in the ephemeris model provides a sufficiently long duration to test stationkeeping capabilities.⁶

Davis et al. have investigated stationkeeping capabilities on the transition halo orbits using the conventional x -axis control approach, with a single maneuver per orbit near the apoapsis, one that targets the rotating \dot{x} value at certain xz -plane crossings further downstream.⁶ It is observed that, using the approach, only certain baseline solutions are conducive to long-term orbit maintenance. In addition, simulations for orbit determination errors larger than 3σ of 0.3 km and 0.3 cm/s, resulted in trajectories diverging from the virtual reference solution, and consequently produced fewer successful stationkeeping cases. Similar results are observed in this investigation as well. Upon careful observation, it is clear that the position and velocity states along the transition halo orbits are sensitive to epoch dates and, therefore, stationkeeping operations must also target the necessary timing conditions at the corresponding epochs, i.e., the actual trajectory must be in phase with the baseline trajectory.

Phase-control The conventional x -axis control approach is effective in low-cost orbit maintenance of the spacecraft in the vicinity of a virtual baseline solution. Since only two of the seven states are targeted, y and \dot{x} quantities, the ample flexibility in the targeting algorithm results in the spacecraft remaining loosely bounded in the neighborhood of the virtual reference trajectory at a relatively low-cost. However, the actual spacecraft trajectory that incorporates the low-cost impulsive

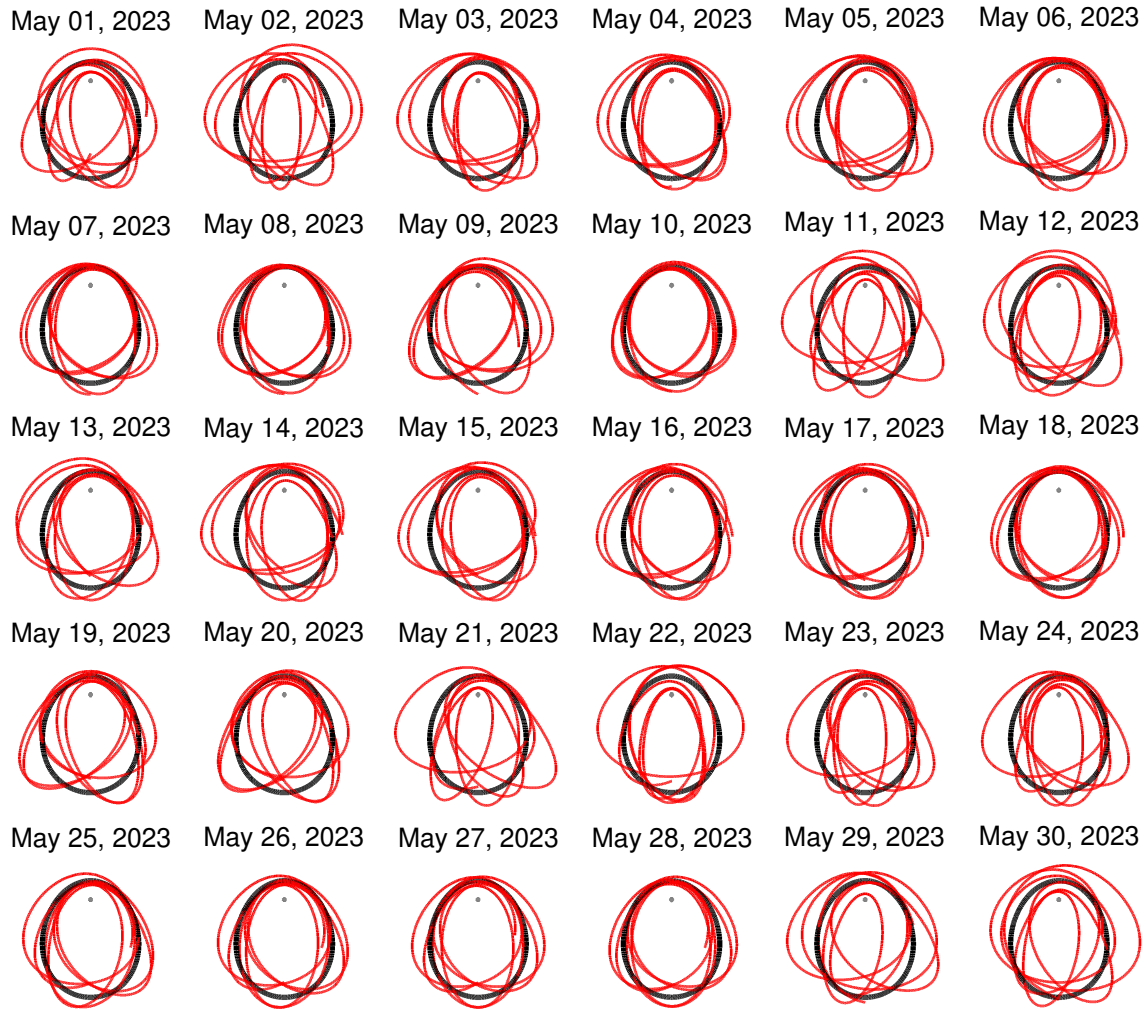


Figure 12: L2 NRHO with perilune radius 15000 km in CR3BP (black) and higher-fidelity ephemeris model (red) converged for different starting epoch dates in May 2023. All projections are in yz view; trajectory direction is clockwise.

stationkeeping maneuvers as produced by the conventional approach does not necessarily synchronize in phase space with the virtual reference trajectory, resulting in lagging or leading the virtual reference in time. In literature, it is observed that the phase difference between the actual spacecraft trajectory and the virtual baseline trajectory increases either positively or negatively over time, when maneuvers are implemented using the conventional x-axis control algorithm.^{10,17} For transition halo orbits that are sensitive to epoch time, any phase shift between the actual and reference trajectories may impede the stationkeeping operations. To overcome such sensitivities, additional constraints are introduced on the impulsive stationkeeping control algorithm to compute maneuvers that deliver appropriate phasing between the actual trajectory and the virtual baseline trajectory. Davis et al.¹⁷ target the rotating \dot{x} value as well as the periapsis altitude simultaneously to maintain appropriate phasing while Muralidharan and Howell¹⁰ use a feedback equation to overcome any phase shift. In any case, if the spacecraft has deviated significantly from a virtual reference trajectory, an occasional long horizon orbit correction maneuver is implemented to shift the states to a new long horizon virtual reference trajectory. In this investigation, the time shift feedback equation

is explored for stationkeeping on the transition halo orbits.

Maintaining appropriate phasing at the periapsis, or the apoapsis, or even the xz -plane crossing are complementary. Since the x -axis control approach targets a condition at the xz -plane crossing, incorporating an additional phase control constraint at the xz -plane crossing is straightforward. To target conditions at the xz -plane crossing that occur at a specific time corresponding to the virtual reference, a fixed time single shooting targeting scheme is incorporated. As demonstrated by Muralidharan and Howell,¹⁰ a feedback constraint is formulated as

$$\Delta y_f - \dot{y}_f \Delta t_0 = [\varphi_{T,24} \quad \varphi_{T,25} \quad \varphi_{T,26}] \Delta \bar{v}_0 \quad (9)$$

that is evaluated along with the conventional x -velocity control equation as in equation (5) to compute a suitable maneuver. The final time of propagation, $t_f = t_{Target} = t_{xz}^*$ is the time along the virtual reference trajectory at the predetermined xz plane crossing. The quantity $\dot{y}_f \Delta t_0$ in equation (9) is the feedback term to compensate for the variation in phase detected at the apoapsis where the maneuver is computed. The term Δy_f corresponds to the change in y position between the actual and the reference trajectory at the end of the propagated trajectory. For a trajectory with no phase difference, $\Delta t_0 = 0$. Using an iterative Newton-Raphson process, the states are iteratively updated with a goal that the left side of equation (9) is equal to zero to within an acceptable tolerance. The maneuver computed with an additional phase constraint keeps the spacecraft motion bounded in the vicinity of the virtual reference trajectory in the time states as well.

A low-cost stationkeeping maneuver is generated typically by targeting further downstream to allow sufficient time to achieve the target conditions. The phase control approach applied on the 3:1 synodic resonant L2 NRHO with perilune radius 15000 km, a reference trajectory that falls within the transition halo orbit range, by targeting the 1st xz -plane crossing near the periapsis is less effective in terms of cost and the number of successful cases compared to targeting the 2nd xz -plane crossings near the periapsis, for both low and high orbit determination levels. Targeting the 2nd xz -plane crossing is successful in maintaining the spacecraft near the virtual reference orbit even with high orbit determination errors (3σ of 10 km and 10 cm/s), which is a considerable improvement compared to the conventional x -axis control algorithm that is effective only for certain virtual reference orbits for very low orbit determination levels with 3σ of 0.3 km and 0.3 cm/s, in position and velocity respectively. Due to the sensitivity of the transition halo orbits, single shooting differential correction process faces a challenge with relatively longer target horizons, such as 6.5 rev downstream.

The sensitivity of the stationkeeping process on a reference orbit is measured by monitoring the stationkeeping performance along two reference orbits of the same NRHO with the same epoch constructed using different approaches. A comparison of annual stationkeeping costs on two set of reference solutions is plotted in Figure 13 for the 3:1 synodic L2 NRHO with perilune radius 15000 km for different epoch dates in the month of May in 2023 described by the x -coordinate. The annual costs are estimated over 100 Monte Carlo simulations, consistent with the cases discussed previously. The set of reference orbits labelled as Sample 1, is generated by stacking 12 revolutions of the CR3BP orbit with 10 patch points along each orbit spaced equally in time, as detailed previously. In contrast, Sample 2 is generated by stacking 25 revolutions of the CR3BP orbit with 10 patch points along each orbit spaced equally in time. In both sample cases, the first node is constrained to be on the xz -plane. Not surprisingly, the stationkeeping cost is sensitive to the virtual reference trajectory. Hence, a direct cost comparison between trajectories constructed on two different epoch dates or using a different sequence of stacking operations, is not practical, as they are based on distinct natural baseline trajectories.

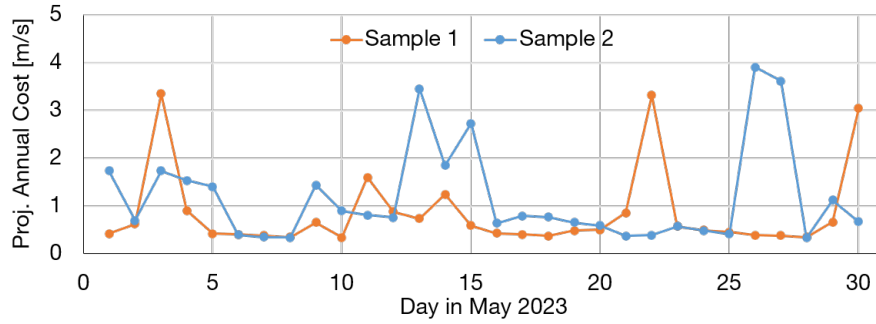
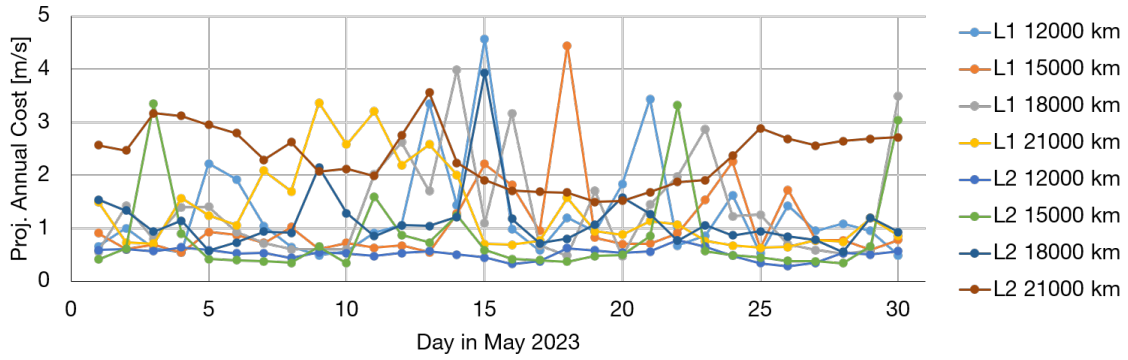


Figure 13: Projected annual stationkeeping cost comparison for reference orbits constructed on same epoch dates through different stacking approaches. Case: 3:1 synodic resonant L2 NRHO with perilune radius 15000 km with low orbit determination error level (3σ : 1km and 1 cm/s).

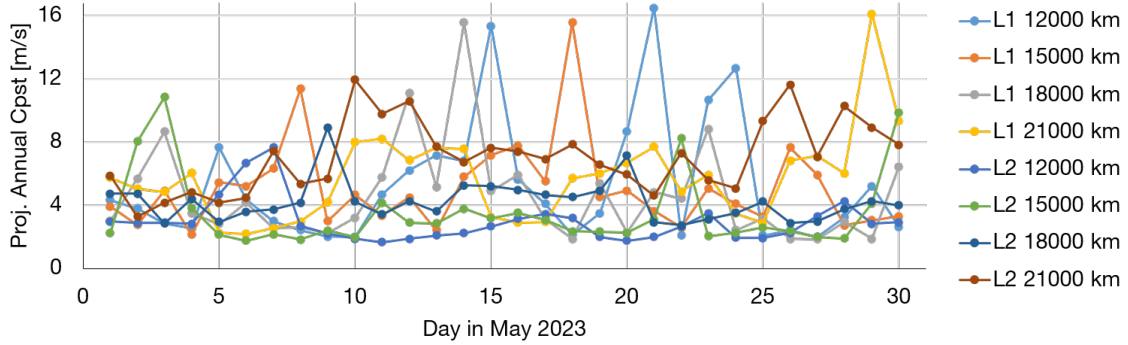
The stationkeeping costs estimated on the transition halo orbit is, of course, impacted by the underlying natural trajectory that serves as the virtual reference trajectory. Although, the mean estimated cost associated with the stationkeeping for a specific trajectory is not very useful, the range of mean stationkeeping costs associated with the same orbit constructed over different epoch dates may yield more relevant details. Figures 14(a) and 14(b) summarizes the projected annual orbit maintenance cost along different halo orbits in the transition region estimated by running 100 Monte Carlo simulations. Each curve represents a transition halo orbit in the L1 and L2 regions. The x -coordinate along these curve represents the epoch date at the halo orbit injection, i.e., the first node of the stacking sequence. The y -coordinate of the curve is the estimated mean stationkeeping costs computed for that epoch date. These simulations are conducted for a mission duration of 90 days. For low orbit determination errors, majority of the stationkeeping simulations across different orbits remains bounded near the virtual reference solutions, simulated over a range of epoch dates in the month of May 2023. A few trajectories do depart from the virtual reference solution. The worst performing case, L2 halo orbit with 21000 km on May 26, 2023, does include at least 80% simulations that remain bounded. In general, the annual stationkeeping cost across different halo orbits are generally in the range between 0.3 m/s and 5 m/s, for low orbit determination errors. In contrast, with higher orbit determination errors, the success rate is at least 60% successful Monte Carlo trials, across different orbits simulated over a range of epoch dates. The worst performing case for high orbit determination errors, the L1 halo orbit with 18000 km on May 13, 2023, includes only 16% Monte Carlo trials that successfully maintain the spacecraft near the virtual reference solution over the mission duration. Again, roughly, annual stationkeeping cost across different halo orbits are typically in the range of 1.5 m/s to 16 m/s, for high orbit determination errors.

CONCLUDING REMARKS

An impulsive stationkeeping technique using the x -axis control strategy is investigated for low-cost orbit maintenance in the low perilune radius NRHOs that offer candidate solutions for various cislunar missions. A straightforward approach is demonstrated that utilizes the interaction between the flow evolving from one maneuver location to the following location during coast segments and the flow evolution from the maneuver location to the target, to identify likely combinations of maneuver and target locations. The cost of stationkeeping operations as well as boundedness of spacecraft trajectory near the virtual reference using the conventional x -axis control approach is correlated to the flow along the corresponding reference orbit. In general, it is an effective strategy to deliver maneuvers that are strategically oriented in a direction away from the most stretching direction. For the L2 NRHOs, stationkeeping maneuvers implemented once per revolution at the



(a) Low orbit determination error (3σ : 1 km and 1 cm/s)



(b) High orbit determination error (3σ : 10 km and 10 cm/s)

Figure 14: Projected annual stationkeeping cost [m/s] for different transition halo orbits in the L1 and L2 regions simulated over a range of epoch dates in May 2023.

apoapsis location by targeting the rotating \dot{x} value at the xz -plane crossing 1.5 rev downstream results in a maneuver that is significantly aligned with the most stretching direction, causing the spacecraft to gradually escape the virtual reference trajectory. In contrast, the maneuver generated by targeting the xz -plane crossing 6.5 rev downstream are aligned away from the most stretching directions, thus efficient and economic. Unlike the L2 NRHOs, a maneuver implemented at the apoapsis does not necessarily produce effective stationkeeping maneuvers for the L1 NRHOs. Nevertheless, several combinations of symmetric and asymmetric maneuver locations along the orbit, with one or more maneuvers per revolution are explored, that are likely suitable for stationkeeping. The halo orbits possessing lunar pass distances such that the orbits in the transition region are sensitive to epoch dates, hence, the conventional x -axis control algorithm that target only the rotating \dot{x} quantity at a specific xz -plane crossing is not effective. By incorporating an additional active phase control constraint, effective stationkeeping maneuvers are delivered. For the transition halo orbits, the annual cost and boundedness of the spacecraft near the virtual baseline trajectory is observed to be dependent on the underlying natural trajectory.

ACKNOWLEDGEMENTS

The authors are grateful the members of the Multi-Body Dynamics Research Group for the insightful discussions. Facilities provided by the School of Aeronautics and Astronautics at Purdue University as well as the Rune and Barbara Eliassen Visualization Laboratory is appreciated. The

work was partly supported by the Purdue University Minority Engineering Program.

REFERENCES

- [1] E. M. Zimovan, K. C. Howell, and D. C. Davis, "Near rectilinear halo orbits and their application in cis-lunar space," *3rd IAA Conference on Dynamics and Control of Space Systems, Moscow, Russia*, 2017, p. 20.
- [2] D. Guzzetti, E. M. Zimovan, K. C. Howell, and D. C. Davis, "Stationkeeping analysis for spacecraft in lunar near rectilinear halo orbits," *27th AAS/AIAA Space Flight Mechanics Meeting, San Antonio, Texas, USA*, February 2017, pp. 1–20.
- [3] G. Gómez, K. Howell, J. Masdemont, and C. Simó, "Station-keeping strategies for translunar libration point orbits," *Advances in Astronautical Sciences*, Vol. 99, No. 2, 1998, pp. 949–967.
- [4] K. C. Howell and T. M. Keeter, "Station-keeping strategies for libration point orbits- Target point and Floquet Mode approaches," *Spaceflight mechanics 1995*, 1995, pp. 1377–1396.
- [5] V. Muralidharan, "Orbit Maintenance Strategies for Sun-Earth/Moon Libration Point Missions: Parameter Selection for Target Point and Cauchy-Green Tensor Approaches," M.S. Thesis, Purdue University, 2017.
- [6] D. C. Davis, S. M. Phillips, K. C. Howell, S. Vutukuri, and B. P. McCarthy, "Stationkeeping and transfer trajectory design for spacecraft in cislunar space," *AAS/AIAA Astrodynamics Specialist Conference, Stevenson, Washington, USA*, August 2017.
- [7] D. Davis, S. Bhatt, K. Howell, J.-W. Jang, R. Whitley, F. Clark, D. Guzzetti, E. Zimovan, and G. Barton, "Orbit maintenance and navigation of human spacecraft at cislunar near rectilinear halo orbits," *27th AIAA Space Flight Mechanics Meeting, San Antonio, Texas, USA*, February 2017.
- [8] D. Folta and F. Vaughn, "A Survey of Earth-Moon Libration Orbits: Stationkeeping Strategies and Intra-Orbit Transfers," *AIAA/AAS Astrodynamics Specialist Conference and Exhibit, Providence, Rhode Island, USA*, August 2004.
- [9] D. Folta, T. Pavlak, K. Howell, M. Woodard, and D. Woodfork, "Stationkeeping of Lissajous trajectories in the Earth-Moon system with applications to ARTEMIS," *AIAA/AAS Astrodynamics Specialist Conference, Toronto, Canada*, August 2010.
- [10] V. Muralidharan and K. C. Howell, "Stationkeeping in Earth-Moon Near Rectilinear Halo Orbits," *AAS/AIAA Astrodynamics Specialist Conference, South Lake Tahoe, California, USA*, August 2020.
- [11] V. Szebehely, "Theory of orbits: the restricted problem of three bodies," tech. rep., Yale univ New Haven CT, 1967.
- [12] K. C. Howell, "Three-dimensional, periodic, 'halo' orbits," *Celestial mechanics*, Vol. 32, No. 1, 1984, pp. 53–71.
- [13] C. Acton, N. Bachman, J. Diaz Del Rio, B. Semenov, E. Wright, and Y. Yamamoto, "Spice: A means for determining observation geometry," *EPSC–DPS Joint Meeting*, 2011.
- [14] T. Pavlak and K. Howell, "Strategy for optimal, long-term stationkeeping of libration point orbits in the Earth-Moon system," *AIAA/AAS Astrodynamics Specialist Conference, Minneapolis, Minnesota, USA*, August 2012.
- [15] V. Muralidharan, A. Weiss, and U. V. Kalabic, "Control Strategy for Long-Term Station-Keeping on Near-Rectilinear Halo Orbits," *30th AIAA/AAS Space Flight Mechanics Meeting, Orlando, FL, USA*, January 2020.
- [16] D. C. Folta, T. A. Pavlak, A. F. Haapala, K. C. Howell, and M. A. Woodard, "Earth–Moon libration point orbit stationkeeping: theory, modeling, and operations," *Acta Astronautica*, Vol. 94, No. 1, 2014, pp. 421–433.
- [17] D. C. Davis, F. S. Khoury, K. C. Howell, and D. J. Sweeney, "Phase Control and Eclipse Avoidance in Near Rectilinear Halo Orbits," *43rd AAS Guidance, Navigation and Control Conference, Breckenridge, CO, United States*, 2020.
- [18] K. C. Howell and S. C. Gordon, "Orbit determination error analysis and a station-keeping strategy for Sun-Earth L1 libration point orbits," *Journal of the Astronautical Sciences*, Vol. 42, 1994, pp. 207–228.
- [19] G. Haller, "Lagrangian coherent structures from approximate velocity data," *Physics of fluids*, Vol. 14, No. 6, 2002, pp. 1851–1861.
- [20] C. R. Short and K. C. Howell, "Lagrangian coherent structures in various map representations for application to multi-body gravitational regimes," *Acta Astronautica*, Vol. 94, No. 2, 2014, pp. 592–607.
- [21] J. S. Subirana, J. J. Zornoza, and M. Hernández-Pajares, "Gnss data processing. volume 1: Fundamentals and algorithms," *ESA Communications ESTEC, PO Box*, Vol. 299, 2013, p. 2200.
- [22] S. Vutukuri, "Spacecraft Trajectory Design Techniques Using Resonant Orbits," M.S. Thesis, Purdue University, 2018.